Reaction mechanism and kinetics of Criegee intermediate and hydroperoxymethyl formate

Meifang Chen [1,2], *Shengrui Tong* [2,*], *Zhen Wang* [2,3], *Weiran Li* [2,3],
Yanyong Xu [1], *Sufan Wang* [1,*], *Maofa Ge* [2,3,4]

[1] *College of Chemistry and Material Science, Anhui Normal University, Wuhu 241000, China*
[2] *State Key Laboratory for Structural Chemistry of Unstable and Stable Species, Chinese Academy of Sciences Research/Education Center for Excellence in Molecular Sciences, Institute of Chemistry, Chinese Academy of Sciences, Beijing 100190, China*
[3] *Center for Excellence in Regional Atmos. Environ., Institute of Urban Environment, Chinese Academy of Sciences, Xiamen 361021, China*
[4] *University of Chinese Academy of Sciences, Beijing 100049, China*

ARTICLE INFO

ABSTRACT

The reaction mechanism and kinetics of the simplest Criegee intermediate CH_2OO reaction with hydroperoxymethyl formate (HPMF) was investigated at high-level quantum chemistry calculations. HPMF has two reactive functional groups, -C(O)OH and -OOH. The calculated results of thermodynamic data and rate constants indicated that the insertion reactions of CH_2OO with –OOH group of HPMF were more favorable than the reactions of CH_2OO with -C(O)OH group. The calculated overall rate constant was 2.33×10^{-13} cm^3/(molecule·sec) at 298 K and the rate constants decreased as the temperature increased from 200 to 480 K. In addition, we also proved the polymerization reaction mechanism between CH_2OO and -OOH of HPMF. This theoretical study interpreted the previous experimental results, and supplied the structures of the intermediate products that couldn't be detected during the experiment.

© 2021 The Research Center for Eco-Environmental Sciences, Chinese Academy of Sciences. Published by Elsevier B.V.

Introduction

Alkenes are one of the most abundant volatile organic compounds (VOCs) in the atmosphere, and can be ozonized to form carbonyl oxides, Criegee intermediates (CIs) (Alam et al., 2011; Johnson and Marston, 2008; Li et al., 2020, 2018; Zeng and Wilson, 2020). Vibrationally excitation of partial CIs can undergo unimolecular decomposition to yield the hydroxyl radicals, OH (Barber et al., 2020; Lester and Klippenstein, 2018; Long et al., 2019; Neeb and Moortgat, 1999; Novelli et al., 2014).

The rest CIs collide with each other or a bath gas (e.g. N_2) to form stabilized Criegee intermediates (sCIs), which can react fast with various trace species in the atmosphere such as water, water dimers, SO_2, NO_x, etc. (Chhantyal-Pun et al., 2020; Liu et al., 2017; Mauldin et al., 2012; Onel et al., 2020; Ryzhkov and Ariya, 2006; Sarkar and Bandyopadhyay, 2020). The rate constants of sCIs react with water or water dimers are not so high. But due to the high concentration of water and water dimers in the low troposphere, the reactions with water or water dimers are considered to be the dominant sink of sCIs (Ryzhkov and Ariya, 2006). The reaction of

---

* Corresponding authors.
  E-mails: tongsr@iccas.ac.cn (S. Tong), sfwang@ahnu.edu.cn (S. Wang).
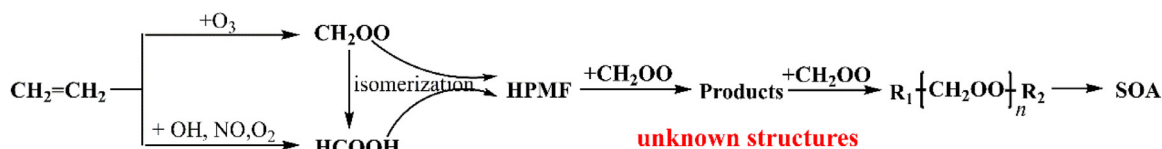
Scheme 1 – Secondary organic aerosols (SOA) formation by ethylene react with ozone. HPMF: hydroperoxymethyl formate, the product of the reaction between CH$_2$OO and HCOOH.

<table>
<tr><td colspan="2">**Table 1 – Reactions of CH$_2$OO that can generated hydroperoxide adducts and the specific structure of the corresponding hydroperoxide adducts.**</td></tr>
<tr><td>Reactions</td><td>Hydroperoxide adducts</td></tr>
<tr><td>CH$_2$OO+H$_2$O
CH$_2$OO+(H$_2$O)$_2$</td><td>HO-CH$_2$OO-H</td></tr>
<tr><td>CH$_2$OO+CH$_3$OH</td><td>CH$_3$O-CH$_2$OO-H</td></tr>
<tr><td>CH$_2$OO+NH$_3$</td><td>NH$_2$-CH$_2$OO-H</td></tr>
<tr><td>CH$_2$OO+HC(O)OH</td><td>HC(O)O-CH$_2$OO-H</td></tr>
</table>

sCIs and water or water dimers can generate hydroxymethyl hydroperoxide (HMHP) (Sheps et al., 2017; Wei et al., 2019). Now more and more scholars are focusing on studying the hydroperoxide adducts produced by CIs oxidation. The reaction of sCIs and this hydroperoxide adducts are considered to be of great significance to the formation of secondary organic aerosol (SOA). Chen et al. (2019) theoretically studied the reaction mechanism and kinetics of several different small sCIs (CH$_2$OO, CH$_3$CHOO, (CH$_3$)$_2$COO) and HMHP. They found that sCIs could polymerize with HMHP and the reaction between sCIs and HMHP was strongly exothermic and spontaneous in the atmosphere (Chen et al., 2019). In addition, sCIs can react with methanol, ethanol (McGillen et al., 2017) and NH$_3$ (Chao et al., 2019) to produce alkoxyalkyl hydroperoxides (AAAH) and hydroperoxamide. However, experimental and theoretical results on this hydroperoxide adduct are still lacking.

The rate constants of sCIs reactions with organic acids are pretty quickly (Chung et al., 2019; Welz et al., 2014). CH$_2$OO is the simplest and the most studied sCIs, which is formed in the ozone decomposition of ethylene and terminal alkenes. HC(O)OH is the most important organic acid, and can be produced through oxidation of some VOCs with high content in the atmosphere (e.g. isoprene, β-pinene et al.) (Khan et al., 2018a; Millet et al., 2015). The rate constants $k_{(298\ K)}$ of the CH$_2$OO + HC(O)OH reaction is closed to the collision limit that is the order of ~10^{-10} cm^3/(molecule·sec) (Vereecken, 2017). The reaction rate constant of CH$_2$OO with HCOOH is about ~10^6 times faster than that of CH$_2$OO with water. Specific values for CH$_2$OO and H$_2$O and HCOOH reaction rates are given in **Table S1**. The main product of reaction between CH$_2$OO and HCOOH is hydroperoxymethyl formate (HPMF) (Chhantyal-Pun et al., 2018). Sakamoto et al. (2013) investigated the formation of secondary organic aerosols (SOA) from ethylene ozonolysis. CH$_2$OO, HPMF, an unknown compound (which composed of CH$_2$OO and HPMF), and oligomeric hydroperoxides with CH$_2$OO as a chain unit were detected through mass spectrometer (Sakamoto et al., 2013). Besides, HCOOH can also be produced by oxidation of ethylene and isomerization of CH$_2$OO (Millet et al., 2015). HPMF generated by CH$_2$OO and HCOOH can further react with CH$_2$OO to form products with unknown structures. The products maybe further react with CH$_2$OO to form oligomers which are high molecular weight, low volatility, and high oxidation, promoting secondary organic aerosols (SOA) growth (Qi et al., 2020; Wang et al., 2016). The formation of SOA through ethylene ozonolysis is shown as Scheme 1. Inomata et al. (2014) also detected HPMF in ozone decomposition of ethylene, propylene, isoprene (Inomata et al., 2014; Jia and Xu, 2020). These results suggest that the reaction process represented in Scheme 1 may be widely present in the ozonization process of terminal alkenes. However, the mechanism of CH$_2$OO reacts with HPMF and the components of products are still unknown especially lacking of theoretical research.

Chung et al. (2019) identified two different structures of HPMF via infrared absorption spectroscopy. The structural diagram of the two configurations of HPMF is shown in **Fig. S1**. One structure was an open-form, and is unstable to single molecular degradation. The other was a rigid structure through intramolecular hydrogen bonds. Moreover, CH$_2$OO reacted with HCOOH to generate HPMF with a rigid structure was a barrier-free process theoretically. The rigid structure HPMF was the main product of CH$_2$OO and HCOOH reaction (Chung et al., 2019). In this work, the reaction between HPMF with rigid structure and CH$_2$OO will be studied by quantum chemistry methods. The mechanism of oligomeric hydroperoxides formation by the reaction of CH$_2$OO and HPMF will be deduced. We hope to provide some insight on the contribution of CIs chemistry to SOA formation.

1. Computational details

All of the geometries of reactants, pre-reactive complexes (CPs), transition states (TSs), and products (Ps) involved in this quantum chemistry study were optimized with density functional theory (DFT) at the M06–2X/6-311+G(2df,2p) level. M06-2X functional performs excellently in predicting the noncovalent interactions, thermochemistry of the main groups and this functional has been widely used to study the bimolecular reaction system of CIs in gas phase, which is suitable for this study system (Zhao and Truhlar, 2008a,2008b). Meanwhile, harmonic vibrational frequencies were calculated at the same level of optimization to ensure that each structure was a minimum (NIMAG = 0) or a saddle point (NIMAG = 1) on the potential energy surface. The frequency correction factor 0.98 was used to correct all frequencies. For optimized structures, TSs
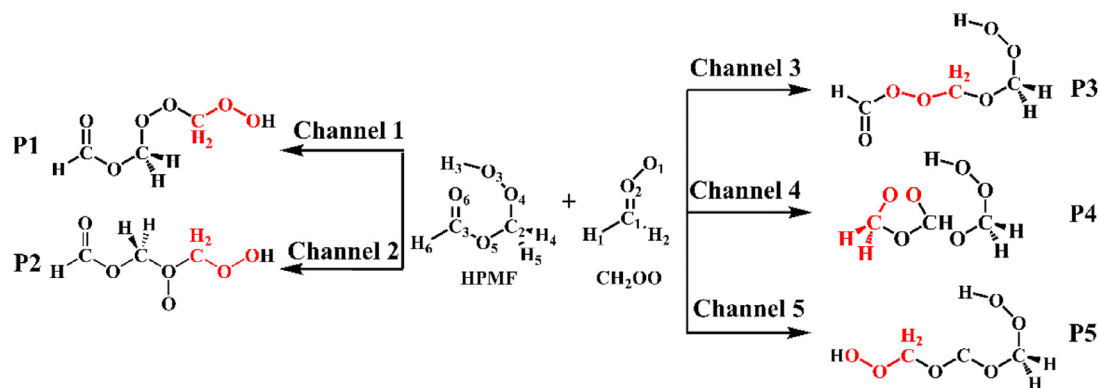
Scheme 2 – Five reaction channels described for the reaction of CH$_2$OO with HPMF and the structure forms of five corresponding products.

were further testified by performing the intrinsic reaction co-ordinate (IRC) calculations which could establish the linkage between reactants and products. To minimize the impact of quantum levels on the energy barriers of the reactions, the single point energy calculated at the M06-2X/def2-TZVP on the basis of geometries optimized at the 6-311+G(2df,2p) and the basis set superposition errors (BSSEs) were taken into account in calculating CPs single point energies (Handy, 2002) The pre-dicted Gibbs free energy was equal to the corrected value of the free energy calculated at M06-2X/6-311+(2df,2p) level plus the electronic energy at M06-2X/def2-TZVP level. The calcu-lation of enthalpy (ΔH) was analogous to that of the Gibbs free energy (ΔH = thermal correction to enthalpy + electronic energy). We compared the thermodynamic data calculated at M06–2X/def2-TZVP//M06-2X/6-311+(2df,2p) with the ther-modynamic data obtained by CCSD(T)/6-311+G(2df,2p)/M06–2X/6-311+G(2df,2p) to verify the correctness of our method. Specific descriptions can be found in **Table S2**. All opera-tions on DFT were performed by Gaussian 16 program suite (Frisch et al., 2016). The reduced density gradient (RDG) has been widely used to study medium and long-term effects (Johnson et al., 2010), and was adopted to reflect the weak in-teraction areas involved in the system by Multiwfn program (Lu and Chen, 2012) and gnuplot visual molecular dynamics (VMD) software (Humphrey et al., 1996) to further prove the in-tramolecular hydrogen bonding in reactants and pre-reactive complexes.

Finally, the rate constants of individual channels in the re-action CH$_2$OO + HPMF were calculated based on the ener-gies predicted at M06-2X/def2-TZVP//M06-2X/6-311+G(2df,2p) level by conventional transition state theory (CTST) with Wigner tunneling correction factor at temperatures between 200 and 380 K. The reaction between CH$_2$OO and HPMF fol-lowed the mechanism of two-step reaction, and the rate con-stants of reaction channels were obtained by using the steady-state approximation (SSA) method. The detailed discussion is shown below

$$CH_2OO + HCOOCH_2OC(O)H(HPMF) \underset{k_{-1}}{\overset{k_1}{\rightleftharpoons}} CP1 \overset{k_2}{\rightarrow} TS1 \rightarrow P1 \quad (1)$$

where k_1 is the rate constant of the forward reaction from the reactants to the pre-reaction complex, k_{-1} is the reverse

reaction rate constant from the reactants to the pre-reactive complex, k_2 is the rate constant of the reaction from the pre-reactive complex to the transition state, CP1, TS1 and P1 are the pre-reaction complex, transition states and product, re-spectively. As shown in the Eq. (1), if $k_2 \ll k_1$, the overall rate constant is

$$k_{over} = \frac{k_1}{k_{-1}}k_2 = \sigma \frac{Q_{CP(T)}}{Q_{R1(T)}Q_{R2(T)}} \exp\left(\frac{G_R - G_{CP}}{RT}\right) \quad (2)$$

where σ is the reaction symmetry number, $Q_{CP(T)}, Q_{R1(T)}, Q_{R2(T)}$ are the partition functions of pre-reactive complexes, CH$_2$OO and HPMF, and G_R and G_{CP} are the total Gibbs free energy of reactants and complexes, respectively, T is the temperature in Kelvin, R is molar gas constant.

The tunnel effect is reflected by the transmission coeffi-cient (ξ). The Wigner tunnel effect used in this article is calcu-lated as

$$\xi_{wigner}(T) = 1 + \frac{1}{24}\left((h \times Im(v^{\neq}))/(k_bT)\right)^2 \quad (3)$$

where $Im(v^{\neq})$ is the imaginary frequency of the relevant tran-sition state, k_b is Boltzman's constants, h is the Planck's con-stants. The calculation of the rate constants was completed in KiSThelp (Canneaux et al., 2014).

2.   Results and discussion

CH$_2$OO has zwitterionic properties with positively charged oxygen and negatively charged carbon and can react with two groups (-C(O)OH and -OOH) of HPMF. Five channels proposed for CH$_2$OO and HPMF reaction are shown in Scheme 2. Chan-nels 1 and 2 are the reaction between CH$_2$OO and the -OOH group of HPMF, channel 1 is insertion of CH$_2$OO between O3 and H3 atoms, while channel 2 is insertion of CH$_2$OO between O4 and H3 atmos. Channels 3, 4, and 5 are the reaction path-ways of CH$_2$OO with the –C(O)OH group of HPMF, channel 3 is integrally insertion of CH$_2$OO between C3 and O5, channel 4 is different from other reaction channels and is the cycload-dition reaction of CH$_2$OO with the carbonyl, and channel 5 is insertion of CH$_2$OO between O6 and H6 atoms of HPMF. The mechanism of the five reaction channels will be detailly dis-cussed below.
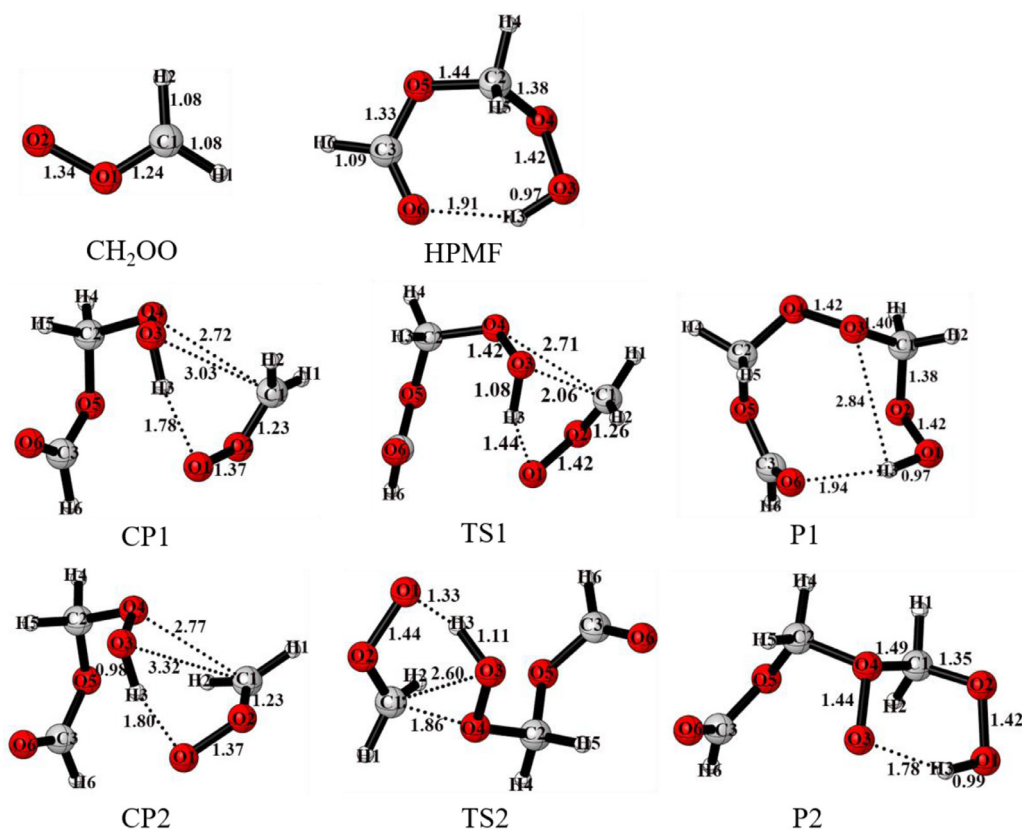
Fig. 1 – Optimized structures of reactants, complexes, transition states and products for channel 1 and 2 at M06-2X/6-311+G(2df,2p). Labeled bond lengths are in angstroms (Å). CP, TS and P are the pre-reaction complex, transition states and product, respectively.

2.1. Reaction channels for CH_2OO and -OOH group of HPMF

Fig. 1 shows the optimized structures of the relevant stationary points involved in channels 1 and 2. As the first step of reaction, CH_2OO approaches to the -OOH group of HPMF from different directions driven by weak interaction to form pre-reactive complexes. As shown in **Fig. S1**, the type of weak interactions by RDG method are demonstrated. Comparing two reactants monomers, the structure of HPMF changes obviously in pre-reactive complexes, namely CP1 and CP2. -C(O)OH- fragment (C3O6O5H6) significantly rotates around C2-O5 bond in the formation process of CP1 and CP2. -C(O)OH-fragment (C3O6O5H6) significantly rotates around C2-O5 bond in the formation process of CP1 and CP2. The reason for this structural change may be when the two reactants are close to each other, the terminal O1 atom of CH_2OO repels with the O6 atom of HPMF, then destroys the original intramolecular hydrogen bonds (O3-H3…O6) of HPMF and generates new hydrogen bond (O3-H3…O1). The hydrogen bond length of CP1 differs from that of CP2 by 0.02 Å (1.78 and 1.80 Å), and the distances between other related atoms are very similar. Therefore, from the structural characteristics, we can infer that the weak interaction of CP1 is a little stronger than CP2. Considering the BEES corrections, the weak interaction energy of CP1 and CP2 is −9.71 and −9.67 kcal/mol at M06-2X/def2-

TZVP//M06-2X/6-311+G(2df,2p) level, respectively. This data is consistent with the structural characteristic analysis.

Follow the reaction direction, two transition states have been located. The distance between the two reactants is further reduced compared to CP1 and CP2. For TS1, the distance of H3-O1, C1-O3, and C1-O4 have lessened to 1.44, 2.06, and 2.71 Å. For TS2, the distance of H3-O1, C1-O3, and C1-O4 have lessened to 1.33, 2.60, and 1.86 Å. To further clarify the reaction mechanism, IRC calculations were performed based on two transition state structures. The changes of main bond length involved in the channel 1 and channel 2 are shown in Fig. 2. Positive charges C1 atom of CH_2OO gradually approaches O3 and O4 atoms of HPMF, and the distance between the H3 and the O1 is gradually decreasing. Hence, the shortening of C1-O3 distance is the most significant relative to the other bonds (C1-O4, H3-O1). Finally, O3 atom separates from H3 atom and leads to the formation of P1. Therefore, the C1-O3 distance is the most important factor influencing channel 1 reactivity. In channel 2, C1-O4 distance variation before the formation of transition state is the most significant, then H3 separates from the O3.

The potential energy surface (PES) of CH_2OO with HPMF of channel 1 and 2 is shown in Fig. 3. In the process of transitioning into products, the pre-reaction complexes must go through TS1 and TS2 with barriers of −3.91 and −3.92 kcal/mol. The energy of P1 is about 45.29 kcal/mol and
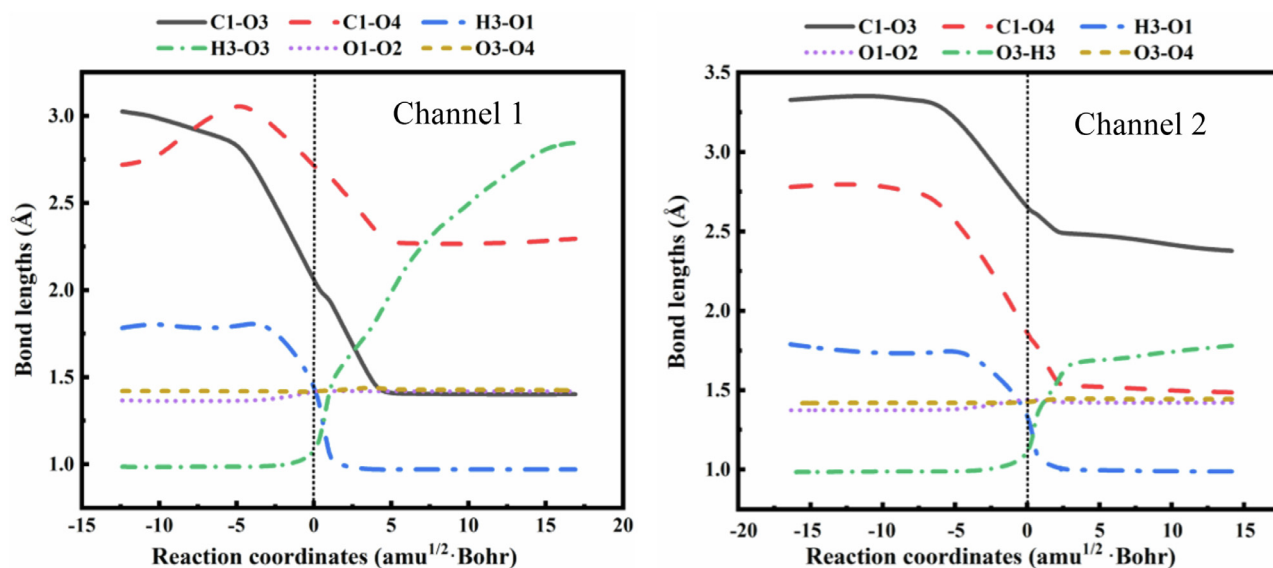
Fig. 2 – Changes in the length of the major bonds along with the reaction coordinates for channels 1 and 2. The zero point in the abscissa corresponds to the bond length of the transition state.
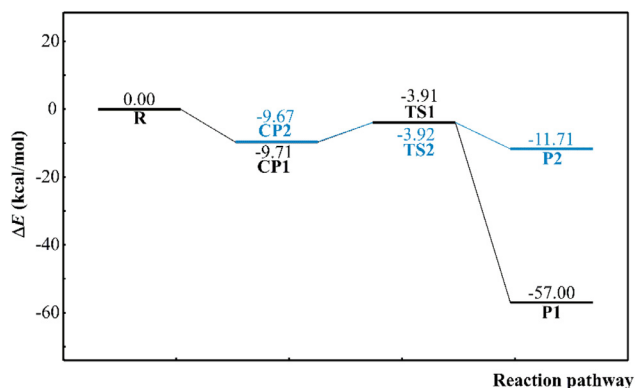

Fig. 3 – Potential energy surfaces (PES, ΔE) for channel 1 and 2 at M06–2X/def2-TZVP//M06-2X/6-311+G(2df,2p). Taking the sum of the two reactant monomers energy as the zero point.

lower than that of P2's, then P1 is structurally more stable. The calculated reaction channels exothermicities are estimated 57.78 and 12.47 kcal/mol, the Gibbs free energy changes are −44.81 and −0.32 kcal/mol for channel 1 and 2. Thus, the above all result shows that channels 1 and 2 are spontaneous and exothermic reactions, which are thermodynamically feasible.

2.2. Reaction channels for CH_2OO and -C(O)OH group of HPMF

Fig. 4 lists the structures of the compounds, transition states, and products involved in channels 3, 4, and 5. For the three reaction channels, CH_2OO approaches to the -C(O)OH group of HPMF from different directions, two CPs have been identified. The complex of channel 3 is labeled CP3, and that of channels 4 and 5 are same which labeled CP4. Different from CP1 and CP2, CP3 and CP4 cannot form a new strong hydro-gen bond (O3-H3…O1). Therefore, CP3 and CP4 weak interaction force is not as strong as CP1 and CP2, which can be further demonstrated by the following thermodynamic data and RDG method (Fig. S1). In CP3, the distances of C3-O1 and C1-O5 have shortened to 2.05 and 1.88 Å, and the bond length of C3-O5 has elongated to 1.43 Å. In CP4, the distance of C1-O6 (2.69 Å), C3-O1 (2.62 Å), H6-O1 (2.86 Å) have shortened compared to the two individual reactants. The distance between CH_2OO and HPMF in the two complexes is quite different, so their weak interaction energy is also different. At M06–2X/def2-TZVP//M06-2X/6-311+G(2df,2p) level, calculated interaction energy of CP3 and CP4 are −4.0 and −7.8 kcal/mol.

As the reactions proceeding, three transition states have been determined. TS3 has a characteristic virtual frequency vibration of −395.9 cm^{-1} which is stretching vibration of C1-O5, C3-O1, C3-O5. Compared to CP3, the distances of C3-O1 and C1-O5 are further reduced to 2.05 and 1.88 Å, and the distance of C3-O5 is further expanded to 1.43 Å. The virtual frequency (−379.4 cm^{-1}) vibration mode of TS4 is the stretching vibration of C1-O6 (2.12 Å), C3-O1 (2.05 Å), and C3-O6 (1.24 Å) bond. TS5's normal vibration mode of virtual frequency is stretching vibration of C3-H6, H6-O1 and C1-O6.

Furthermore, IRC has been established basis on the transition state structure, changes in the associated structural parameters during the reaction are shown in the Fig. 5. In channel 3, the bond length of C1-O5 and O3-O1 are continuously shortened before reaching the transition state as the reaction proceeds. The change of C1-O5 bond length is more obvious than that of C3-O1 bond length. Therefore, the shortening of C1-O5 bond length is the main factor to control the reaction. During the formation of the transition state to the product, the bond length of the C3-O5 gradually becomes longer. The change of bond length of O1-O2 and O3-O4 are not obvious during the whole reaction process. For the change of bond length in the reaction channel 4 and channel 5, we use the same method to analyze and find that the main control
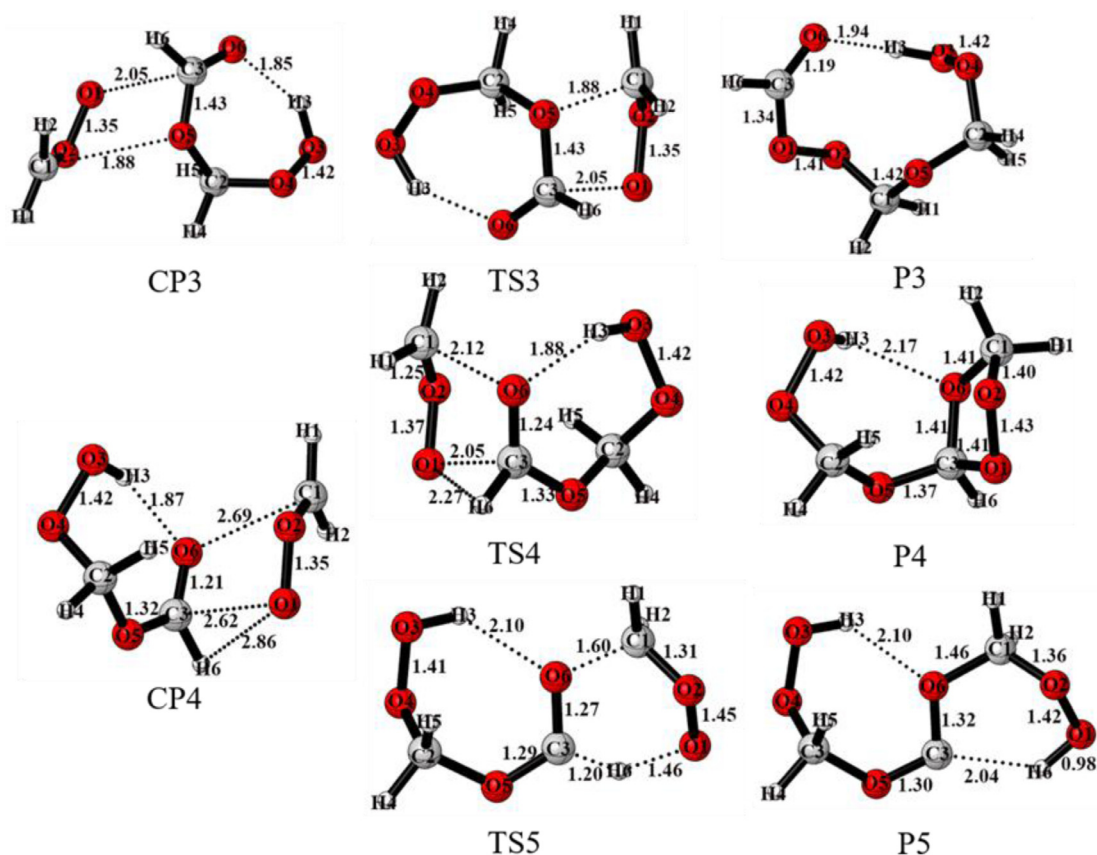
Fig. 4 – Optimized structures of reactants, CPs, TSs and Ps for channel 3, 4 and 5 at M06-2X/6-311+G(2df,2p). Labeled bond lengths are in angstroms. Among them, RC4 is the common complex structure of channels 4 and 5.

function of channel 4 in the reaction process is the shortening of C1-O5 bond length. With respect to channel 5, the change of O1-H6 bond length before the formation of the transition state is the most significant, and the increase of C3-H6 bond length is mainly after the formation of the transition state.

The differences of electronic energies for all stationary points are shown in Fig. 6. Obviously, relative to the energy barriers of the reactants, the energy barrier of TS3 is the highest at 11.25 kcal/mol, the energy barrier of TS5 is 6.68 kcal/mol, and the energy barrier of TS4 is the lowest that is the negative value, −3.23 kcal/mol. The energy barriers of channels 3 and 5 are too high relative to channel 4, and they are not easy to occur. In addition, the Gibbs free energy of channel 4 is −42.29 kcal/mol, and the heat released by the reaction is −55.37 kcal/mol, indicating that reaction channel 4 is thermodynamically favorable.

Based on the discussion in the previous part, channels 1, 2, and 4 are easier to occur among the five reaction channels, and channel 2 has the lowest potential barrier. Thus, the most favorable channel is CH_2OO insertion the H3 and O4 atom of –OOH group in HPMF (namely channel 2). Therefore, we mainly focus on the three reaction channels in the next part.

2.3. Kinetics

The rate constants of channel 1, 2 and 4 are computed using conventional transition state theory (CTST) with Wigner tunneling correction factor from 200 to 380 K at M06-2X/def2-TZVP//M06-2X//6-311+G(2df,2p) level. Chen et al. (2019) previously used the same method to calculate the reaction rate constants when studying kinetics of CIs reactions with hydroxylalkyl hydroperoxides. And they proved the reliability of this method to study similar reactions of CIs with hydroperoxide adducts (Chen et al., 2019). Therefore, this method is also applicable to our research system.

The data in Table 2 shows reaction rate constants of channels 1, 2, and 4. Channel 2 has the fastest reaction rate with 1.73×10^{-13} cm^3/(molecule·sec) under 298 K and 1 atm conditions, and the kinetics results are consistent with that of thermodynamic analysis. The reaction rate constants of channels 1, 2 and 4 are negatively correlated with the increasing of temperature, indicating that the reaction is more likely to occur at low temperature.

Furthermore, the branch ratios of each reaction channels are calculated that based on rate constants. The branching radio which accounts for the individual contribution of the reaction channels to the overall reaction rate is calculated by following expression:

$$\text{Branching radio} = \frac{k_i}{k_{overall}} \times 100\% \tag{4}$$

where k_i is the rate constant of the individual reaction channel, $k_{overall}$ is the sum of rate constants of channels 1, 2, and 4. As the result, the overall rate constants is
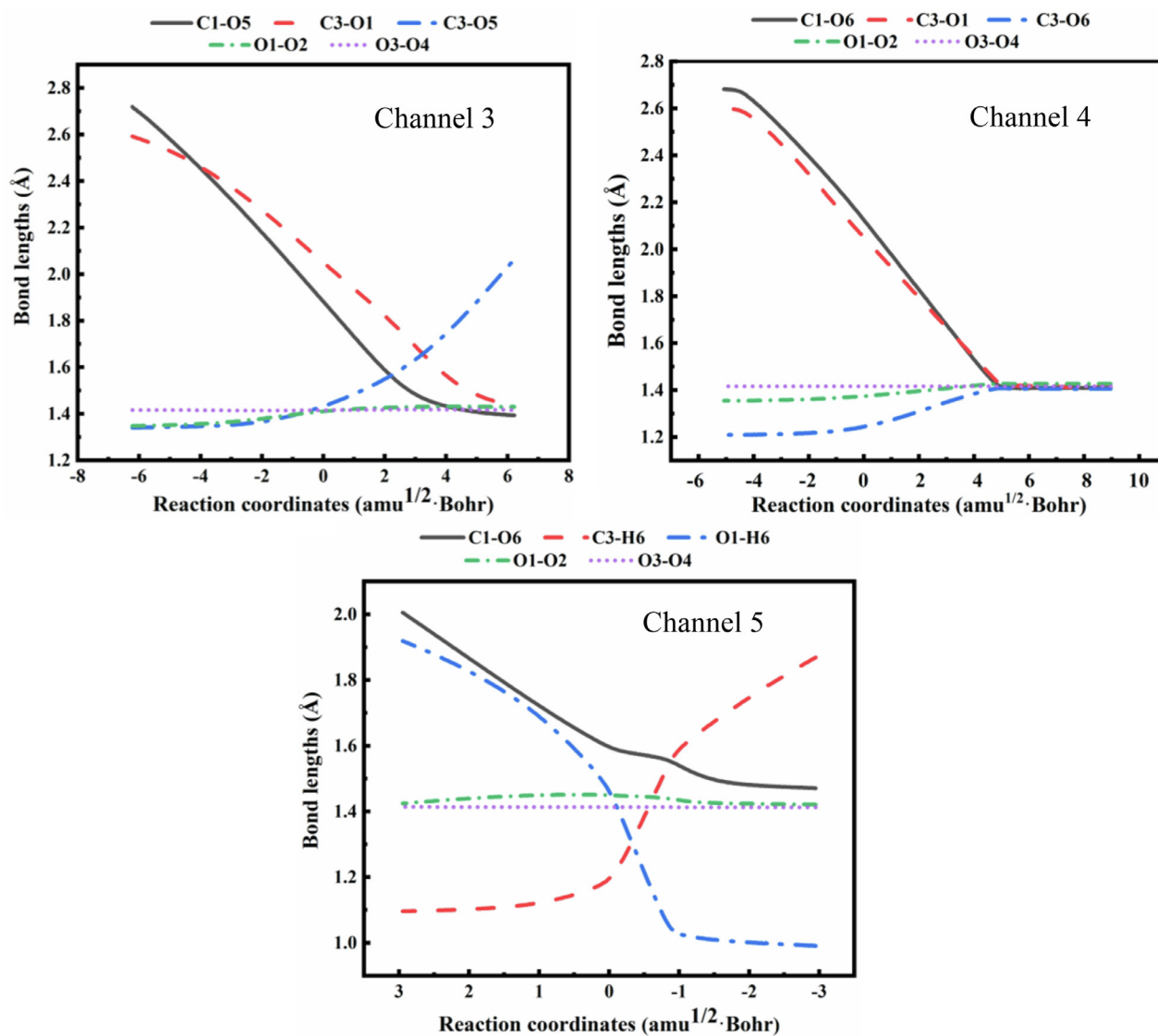
Fig. 5 – Changes in the length of the major bonds along with the reaction coordinates for channel 3, 4 and 5. The zero point in the abscissa corresponds to the bond length of the transition state.

Table 2 – Rate constants for the three main reaction channels from 200 to 480 K at M06-2X/def2-TZVP//M06-2X/6-311+G(2df,2p) level. k_{c1} represents the rate constants of channel 1, k_{c2} represents the rate constants of channel 2, and k_{c4} represents the rate constants of channel 4.

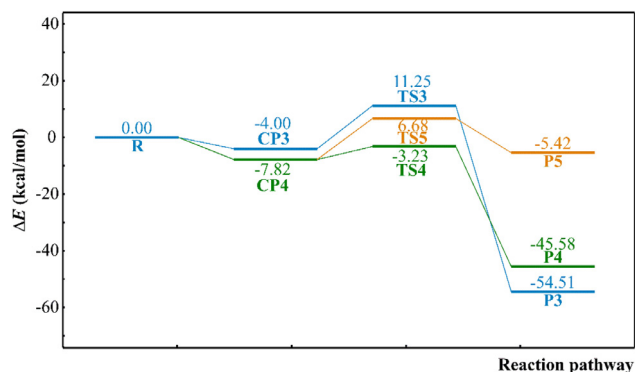| T (K)	k_{c1} (cm³/(molecule·sec))	k_{c2} (cm³/(molecule·sec))	k_{c4} (cm³/(molecule·sec))
200	6.04×10^{-13}	2.74×10^{-12}	2.21×10^{-14}
220	3.01×10^{-13}	1.25×10^{-12}	1.58×10^{-14}
240	1.71×10^{-13}	6.56×10^{-13}	1.21×10^{-14}
260	1.07×10^{-13}	3.84×10^{-13}	9.83×10^{-15}
273	8.20×10^{-14}	2.84×10^{-13}	8.77×10^{-15}
298	5.33×10^{-14}	1.73×10^{-13}	7.33×10^{-15}
320	3.89×10^{-14}	1.20×10^{-13}	6.49×10^{-15}
340	3.06×10^{-14}	9.06×10^{-14}	5.94×10^{-15}
360	2.48×10^{-14}	7.08×10^{-14}	5.54×10^{-15}
380	2.07×10^{-14}	5.72×10^{-14}	5.24×10^{-15}

Fig. 6 – PES for channel 3, 4 and 5 at M06-2X/def2-TZVP//M06–2X/6-311+G(2df,2p). Taking the sum of two reactant monomers energy as the zero point.

2.33×10^{-13} cm^3/(molecule·sec), P2 is the main product of the reaction, and the yield is about 73.93% of the total product at 298 K and 1 atm. According to the formula of the branching ratio, the branching ratio of products is positively correlated with the reaction rate constant of each reaction channel. So for channels 1, 2 and 4, the branching ratio of the corresponding products also decreases with increasing temperature. We still lack the concentration of HPMF in the atmosphere to derive the atmospheric life of HPMF from the reaction rate. In the calculation, some approximations are used to obtain the atmospheric life of HPMF (2.42 hr), as detailed in Appendix A. Supplementary data.

2.4. Formation of oligomeric hydroperoxide

Combining the thermodynamic and kinetic analyses, we can see that CH$_2$OO reacts with -OOH of HPMF is thermodynamically and kinetically feasible and it is more easily than CH$_2$OO reacts with -C(O)OH. The products P1, P2, and P4 of channels 1, 2, and 4 have the same group -OOH as HPMF. Therefore, CH$_2$OO may be further react with -OOH group of P1, P2 and P4 to form oligomers. Theoretically, the reaction of CH$_2$OO with -OOH groups of P1, P2 and P4 are calculated to search the possibility oligomerization. The mechanism is similar as previous channel 1 and 2. The potential energy surfaces of the six channels are shown in Fig. 7. Different from previous analysis, the two channels of P2 react with CH$_2$OO only have one pre-reactive complexes. The mainly reason is that the new hydrogen bonds formed by the two reaction channels are in the same direction. Compared to the channels formed P1 and P2, the energy barriers of the secondary insertion reactions of P1 and P2 are increased to 1.62–5.22 kcal/mol. The channel of P9 formation has the highest energy barrier, 1.26 kcal/mol which means that the reaction channel is more difficult to occur than the other channels. Compared to the channel formed P4, the energy barriers of the two channels of forming P10 and P11 are decreased. The channels formed P6, P8 and P10 are more strongly exothermic than the channels formed P5, P7 and P9. This phenomenon is closely related to the stability of products. P5, P7 and P9 formed ether oxydic groups with higher oxidation properties and may react easily with other trace gases.
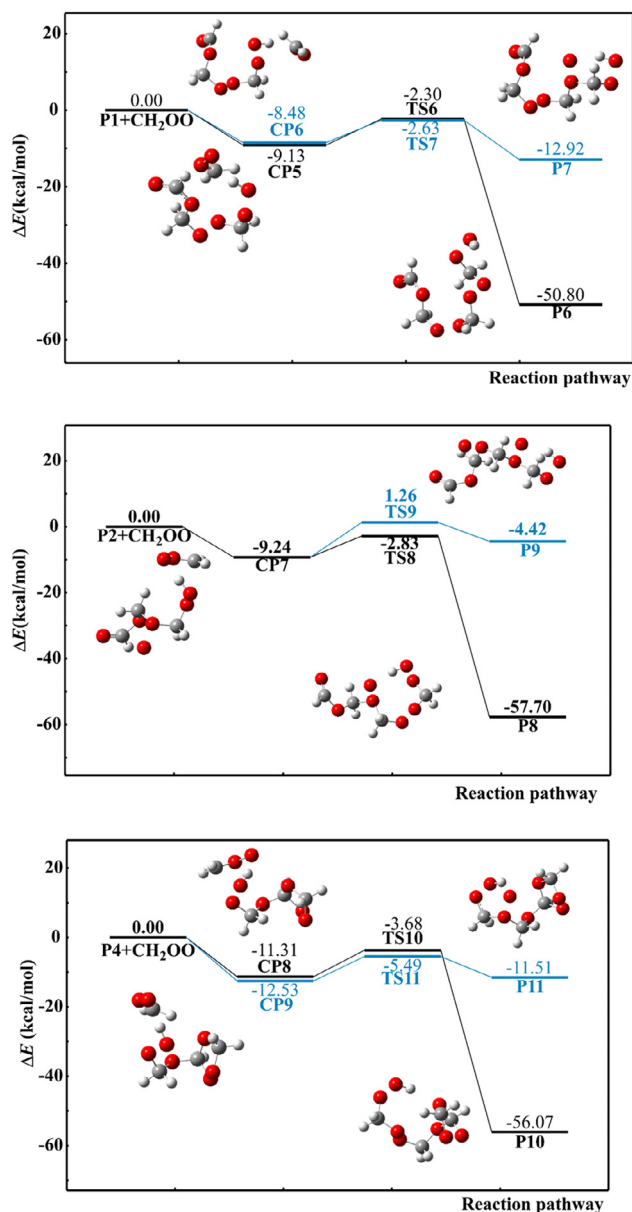

Fig. 7 – PES for CH$_2$OO further reacts with –OOH group of P1, P2 and P4 at M06-2X/def2-TZVP//M06-2X/6-311+G(2df,2p).

The products of secondary oxidation, P6-P10, still had the -OOH groups and could continue to react. Therefore, we considered that CH$_2$OO could polymerize with the -OOH group to produce a polymer with CH$_2$OO as a chain unit.

3. Conclusions and atmospheric implications

The reaction of CH$_2$OO with the HPMF were studied by quantum chemistry method. Five possible reaction channels were proposed. The insert reaction of the -OOH group in HPMF to CH$_2$OO is easier to happen than the –C(O)OH group pathway, which are confirmed by thermochemically and dynamically results. P1, P2 and P4 are the main products of CH$_2$OO reaction with HPMF. The concentration of HPMF in the atmosphere

can reach the ppt level according to the results of model simulation (Khan et al., 2018b), and maybe underestimated as there are still many unknown sources for both CH_2OO and HCOOH (HPMF is the main product of the reaction of CH_2OO and HCOOH). Also, early studies suggested HPMF was a crucial intermediate formed during the oxidation of dimethyl ether (DME) (Andersen and Carter, 2003, 2006; Xing et al., 2015). There is still a lack of HPMF concentration measurement data in the actual observation. Previous studies have been carried out to study the degradation of HPMF by theoretical methods. Compared with the bimolecular reaction discussed in this study, the degradation of HPMF has higher energy barrier (Genossar et al., 2020; Xing et al., 2015). HPMF has a rigid structure, and the occurrence of monomolecular degradation means that intramolecular hydrogen bonding must be overcome first (Chung et al., 2019). Therefore, the reaction of HPMF with CH_2OO is more possible to happen.

The calculated rate constant of CH_2OO react with HPMF is 2.33×10^{-13} cm^3/(molecule·sec) at 298 K and 1 atm. In addition, we find that CH_2OO could polymerize with -OOH group of HPMF. This polymerization is also thermodynamically feasible. Based on the results of this work, we can also predict the specific structure of CH_2OO chain products produced by ethylene ozonolysis observed in the experiment. In forest areas with high concentrations of end- alkene and ozone, this reaction is likely to occur. This reaction mechanism may also be suitable for other larger sCIs. Concentrations of sCIs reached 10^5 cm^{-3} in areas with high emissions of unsaturated hydrocarbons (e.g. Amazon Forest Region) (Khan et al., 2018b). In addition to the product HPMF from reaction between CH_2OO and HCOOH, CH_3CHOO and CH_3COOH can react to generate hydroperoxyethyl acetate (HPEA), and $(CH_3)_2COO$ and CH_3CH_2COOH can react to generate hdroperoxyisopropyl isobutylrate (HPII). HPEA and HPII have the same functional groups with HPMF, and the reaction mechanisms studied by this work are also applicable to the similar type of hydroperoxy compounds. The sufficient sCIs can be polymerized with these hydroperoxides in the troposphere and further significant contribute to SOA formation.

Acknowledgments

Appendix A. Supplementary data

Supplementary material associated with this article can be found in the online version at doi:10.1016/j.jes.2020.12.029.

REFERENCES

Alam, M.S., Camredon, M., Rickard, A.R., Carr, T., Wyche, K.P., Hornsby, K.E., et al., 2011. Total radical yields from tropospheric ethene ozonolysis. Phys. Chem. Chem. Phys. 13, 11002–11015.

Andersen, A., Carter, E.A., 2003. Hybrid density functional theory predictions of low-temperature dimethyl ether combustion pathways. II. Chain-branching energetics and possible role of the Criegee intermediate. J. Phys. Chem. A 107, 9463–9478.

Andersen, A., Carter, E.A., 2006. Insight into selected reactions in low-temperature dimethyl ether combustion from Born–Oppenheimer molecular dynamics. J. Phys. Chem. A 110, 1393–1407.

Barber, V.P., Esposito, V.J., Trabelsi, T., Hansen, A.S., McHenry, T.A., Francisco, J.S., et al., 2020. Experimental and computational investigation of vinoxy and 1-methylvinoxy radicals from the unimolecular decay of alkyl-substituted Criegee intermediates. Chem. Phys. Lett. 751, 7.

Chao, W., Yin, C., Takahashi, K., Lin, J.J-M., 2019. Effects of water vapor on the reaction of CH_2OO with NH_3. Phys. Chem. Chem. Phys. 21, 22589–22597.

Canneaux, S., Bohr, F., Henon, E., 2014. KiSThelP: a program to predict thermodynamic properties and rate constants from quantum chemistry results. J. Comput. Chem. 35, 82–93.

Chen, L., Huang, Y., Xue, Y., Shen, Z., Cao, J., Wang, W., 2019. Mechanistic and kinetics investigations of oligomer formation from Criegee intermediate reactions with hydroxyalkyl hydroperoxides. Atmos. Chem. Phys. 19, 4075–4091.

Chhantyal-Pun, R., Khan, M.A.H., Taatjes, C.A., Percival, C.J., Orr-Ewing, A.J., Shallcross, D.E., 2020. Criegee intermediates: production, detection and reactivity. Int. Rev. Phys. Chem. 39, 383–422.

Chhantyal-Pun, R., Rotavera, B., McGill en, M.R., Khan, M.A.H., Eskola, A.J., Caravan, R.L., et al., 2018. Criegee intermediate reactions with carboxylic acids: a potential source of secondary organic aerosol in the atmosphere. ACS Earth Space Chem. 2, 833–842.

Chung, C.A., Su, J.W., Lee, Y.P., 2019. Detailed mechanism and kinetics of the reaction of Criegee intermediate CH_2OO with HCOOH investigated via infrared identification of conformers of hydroperoxymethyl formate and formic acid anhydride. Phys. Chem. Chem. Phys. 21, 21445–21455.

Frisch, M.J., Trucks, G.W., Schlegel, H.B., Scuseria, G.E., Robb, M.A., Cheeseman, J.R., et al., 2016. Gaussian 16 Rev. A.03 package, Wallingford, C.T.

Genossar, N., Porterfield, J.P., Baraban, J.H., 2020. Decomposition of the simplest ketohydroperoxide in the ozonolysis of ethylene. Phys. Chem. Chem. Phys. 22, 16949–16955.

Handy, N.C., 2002. The calculation of small molecular interactions by the differences of separate total energies. Some procedures with reduced errors - Comment. Mol. Phys. 100, 63.

Humphrey, W., Dalke, A., Schulten, K., 1996. VMD: visual molecular dynamics. J. Mol. Grap. Model. 14, 33–38.

Inomata, S., Sato, K., Hirokawa, J., Sakamoto, Y., Tanimoto, H., Okumura, M., et al., 2014. Analysis of secondary organic aerosols from ozonolysis of isoprene by proton transfer reaction mass spectrometry. Atmos. Environ. 97, 397–405.

Jia, L., Xu, Y., 2020. The role of functional groups in the understanding of secondary organic aerosol formation mechanism from α-pinene. Sci. Total Environ. 738. 139831.

Johnson, D., Marston, G., 2008. The gas-phase ozonolysis of unsaturated volatile organic compounds in the troposphere. Chem. Soc. Rev. 37, 699–716.

Johnson, E.R., Keinan, S., Mori-Sanchez, P., Contreras-Garcia, J., Cohen, A.J., Yang, W., 2010. Revealing Noncovalent Interactions. J. Am. Chem. Soc. 132, 6498–6506.

Khan, M.A.H., Lyons, K., Chhantyal-Pun, R., McGillen, M.R., Caravan, R.L., Taatjes, C.A., et al., 2018a. Investigating the tropospheric chemistry of acetic acid using the global 3-D chemistry transport model, STOCHEM-CRI. J. Geophys. Res.-Atmos. 123, 6267–6281.

Khan, M.A.H., Percival, C.J., Caravan, R.L., Taatjes, C.A., Shallcross, D.E., 2018b. Criegee intermediates and their impacts on the troposphere. Environ. Sci.-Proc. Imp. 20, 437–453.

Lester, M.I., Klippenstein, S.J., 2018. Unimolecular decay of Criegee intermediates to OH radical products: prompt and thermal decay processes. Accounts Chem. Res. 51, 978–985.

Li, W., Chen, M., Chen, Y., Tong, S., Ge, M., Guo, Y., et al., 2020. Kinetic and mechanism studies of the ozonolysis of three unsaturated ketones. J. Environ. Sci. 95, 23–32.

Li, W., Chen, Y., Tong, S., Guo, Y., Zhang, Y., Ge, M., 2018. Kinetic study of the gas-phase reaction of O_3 with three unsaturated alcohols. J. Environ. Sci. 71, 292–299.

Liu, Y., Liu, F., Liu, S., Dai, D., Dong, W., Yang, X., 2017. A kinetic study of the CH_2OO Criegee intermediate reaction with SO_2, $(H_2O)(2)$, CH_2I_2 and I atoms using OH laser induced fluorescence. Phys. Chem. Chem. Phys. 19, 20786–20794.

Long, B., Bao, J.L., Truhlar, D.G., 2019. Rapid unimolecular reaction of stabilized Criegee intermediates and implications for atmospheric chemistry. Nat. Commun. 10, 2003.

Lu, T., Chen, F., 2012. Multiwfn: a multifunctional wavefunction analyzer. J. Comput. Chem. 33, 580–592.

Mauldin III, R.L., Berndt, T., Sipilae, M., Paasonen, P., Petaja, T., Kim, S., et al., 2012. A new atmospherically relevant oxidant of sulphur dioxide. Nature 488, 193–196.

McGillen, M.R., Curchod, B.F.E., Chhantyal-Pun, R., Beames, J.M., Watson, N., Khan, M.A.H., et al., 2017. Criegee intermediate–alcohol reactions, a potential source of functionalized hydroperoxides in the atmosphere. ACS Earth Space Chem 1, 664–672.

Millet, D.B., Baasandorj, M., Farmer, D.K., Thornton, J.A., Baumann, K., Brophy, P., et al., 2015. A large and ubiquitous source of atmospheric formic acid. Atmos. Chem. Phys. 15, 6283–6304.

Neeb, P., Moortgat, G.K., 1999. Formation of OH radicals in the gas-phase reaction of propene, isobutene, and isoprene with O^{-3}: yields and mechanistic implications. J. Phys. Chem. A 103, 9003–9012.

Novelli, A., Vereecken, L., Lelieveld, J., Harder, H., 2014. Direct observation of OH formation from stabilised Criegee intermediates. Phys. Chem. Chem. Phys. 16, 19941–19951.

Onel, L., Blitz, M., Seakins, P., Heard, D., Stone, D., 2020. Kinetics of the gas phase reactions of the Criegee intermediate CH_2OO with O_3 and IO. J. Phys. Chem. A 124, 6287–6293.

Qi, X., Zhu, S., Zhu, C., Hu, J., Lou, S., Xu, L., et al., 2020. Smog chamber study of the effects of NOx and NH_3 on the formation of secondary organic aerosols and optical properties from photo-oxidation of toluene. Sci. Total Environ. 727, 138632.

Ryzhkov, A.B., Ariya, P.A., 2006. The importance of water clusters (H_2O), $(n=2,...,4)$ in the reaction of Criegee intermediate with water in the atmosphere. Chem. Phys. Lett. 419, 479–485.

Sakamoto, Y., Inomata, S., Hirokawa, J., 2013. Oligomerization reaction of the Criegee intermediate leads to secondary organic aerosol formation in ethylene ozonolysis. J. Phys. Chem. A 117, 12912–12921.

Sarkar, S., Bandyopadhyay, B., 2020. Singlet (1Deltag) O_2 as an efficient tropospheric oxidizing agent: the gas phase reaction with the simplest Criegee intermediate. Phys. Chem. Chem. Phys. 22, 19870–19876.

Sheps, L., Rotavera, B., Eskola, A.J., Osborn, D.L., Taatjes, C.A., Au., K., et al., 2017. The reaction of Criegee intermediate CH_2OO with water dimer: primary products and atmospheric impact. Phys. Chem. Chem. Phys. 19, 21970–21979.

Vereecken, L., 2017. The reaction of Criegee intermediates with acids and enols. Phys. Chem. Chem. Phys. 19, 28630–28640.

Wang, M., Yao, L., Zheng, J., Wang, X., Chen, J., Yang, X., et al., 2016. Reactions of atmospheric particulate stabilized Criegee intermediates lead to high-molecular-weight aerosol components. Environ. Sci. Technol. 50, 5702–5710.

Wei, W-m., Hong, S., Fang, W-j., Zheng, R-h., Qin, Y-d., 2019. Formation of OH radicals from the simplest Criegee intermediate CH_2OO and water. Theor. Chem. Acc. 138, 13.

Welz, O., Eskola, A.J., Sheps, L., Rotavera, B., Savee, J.D., Scheer, A.M., et al., 2014. Rate coefficients of C1 and C2 Criegee intermediate reactions with formic and acetic acid near the collision limit: direct kinetics measurements and atmospheric implications. Angew. Chem. Int. Edit. 53, 4547–4550.

Xing, Ll-l., Zhang, X-y., Wang, Z-d., Li, S., Zhang, Ll-d., 2015. New insight into competition between decomposition pathways of hydroperoxymethyl formate in low temperature DME oxidation. Chin. J. Chem. Phys. 28, 563–572.

Zeng, M., Wilson, K.R., 2020. Efficient coupling of reaction pathways of Criegee intermediates and free radicals in the heterogeneous ozonolysis of alkenes. J. Phys. Chem. Let. 11, 6580–6585.

Zhao, Y., Truhlar, D.G., 2008a. Density functionals with broad applicability in chemistry. Acc. Chem. Res. 41, 157–167.

Zhao, Y., Truhlar, D.G., 2008b. The M06 suite of density functionals for main group thermochemistry, thermochemical kinetics, noncovalent interactions, excited states, and transition elements: two new functionals and systematic testing of four M06-class functionals and 12 other functionals. Theor. Chem. Acc. 120, 215–241.